J. Phys. B: At. Mol. Opt. Phys. 27 (1994) 5389–5404. Printed in the UK

Elastic scattering and vibrational excitation cross sections for electron collisions with C_2F_6*

T Takagi†§, L Boesten†, H Tanaka† and M A Dillon‡

† Department of Physics, Sophia University, Chiyoda-ku, Kioicho 7-1, Tokyo 102, Japan
‡ Argonne National Laboratory, 9700 S. Cass Avenue, IL 60439, USA

Received 12 July 1994, in final form 23 August 1994

Abstract. Absolute elastic cross sections for e–C_2F_6 collisions have been measured for impact energies of 2 to 100 eV and scattering angles from 10 to 130°. From these, the integrated and momentum transfer cross sections were obtained by extrapolation and numerical integration. Energy loss spectra were measured for vibrational excitation. The vibrational excitation functions show resonances at 4.3 eV and 8.5 eV. By decomposition of the loss spectra and symmetry analysis according to angular correlation theory, the resonances have been assigned to a temporary trapping of the electrons in the a_{2u} (4.3 eV) and e_u (8.5 eV) antibonding orbitals of the molecule.

1. Introduction

Perfluoroalkanes (C_NF_{2N+2}) are an indispensable tool in new plasma processes (e.g. Haond 1992) and many other patent applications (Iriyama and Yasuda 1992). They are used as etching gases (e.g. Senhorst 1991, Miller and Greenberg 1992), as gaseous insulators in discharge switches (e.g. Božin and Goodyear 1968) or even as a source for C^{13} isotopes (Arai *et al* 1984). Especially in the semiconductor industry they are indispensable in the formation or deposition of semiconductor films (e.g. Reinhardt 1992, Op de Beeck *et al* 1992). However, experimental or theoretical studies of the internal reactions of plasmas containing C_2F_6 have not kept pace with their use.

As far as C_2F_6 is concerned, publications include photoabsorption (Lee *et al* 1977, Pirozhnaya *et al* 1985, theory), vibrational absorption by slow electrons (<0.5 eV, Morris *et al* 1983), multiphoton excitation of the ν_5 vibrational mode to dissociate the C_2F_6 (Fisk 1978), measurements of the electron drift velocity and diffusion/mobility ratios in swarm experiments (Naidu and Prasad 1972), attachment measurements in high-pressure swarm experiments (Hunter and Christophorou 1984), estimation of the momentum transfer cross section from previous swarm measurements (Pirgov and Stefanov 1990), and a theoretical simulation of the geometry and the total and C–C bond dissociation energies (Martell and Boyd 1992). Other related publications have reported measurements of inner-shell excitation and electron transmission (Ishii *et al*

* Work supported by a Grant in Aid from the Ministry of Education, Science, and Culture, Japan, and by the US Department of Energy, Office of Energy Research, Office of Health and Environmental Research, under contract W-31-109-Eng-38.
§ Present address: Anelva Co., Fuchuu, Yotsuya 5-8-1, Tokyo, Japan 183.

0953-4075/94/215389+16$19.50

1988) and negative ion formation by dissociative attachment (Spyrou *et al* 1983). This list is not intended to be complete. No experimental data have been reported for vibrationally elastic and inelastic cross sections for $e + C_2F_6$ except for some yet unpublished cross sections over the limited range of 1–10 eV and scattering angles from 20 to 90° (Merz 1993).

Here, we report on low-energy (2–100 eV) elastic electron scattering experiments over an angular range from 10 to 130°, including electron loss spectra for vibrational excitation up to about 0.6 eV loss.

2. Experimental and analytical techniques

2.1. Apparatus

The present electron spectrometer and its use have been described sufficiently in previous publications (e.g. Tanaka *et al* 1990). Its main features are crossed electron and molecular beams, hemispherical monochromators and analysers, computer-driven voltages, and differential pumping of the electron optics. The resolution was about 30 meV. The nozzle, a simple tube ($L = 5$ mm, $D = 0.3$ mm) was kept at slightly elevated temperatures (80–90 °C) throughout the measurements which—at this resolution—will not lead to appreciable rotational broadening because of the small rotational constants (Frisch *et al* 1992) of C_2F_6, i.e. 2.848 and 1.85 GHz or 1.2 and 0.77×10^{-5} eV. Even the much lighter N_2 requires a resolution of 10 meV in order to reveal a broad rotational structure in energy-loss measurements (Buckley 1977). Similarly, no rotational broadening of the elastic peak could be observed. At 90 °C or an equivalent energy of 31 meV, lower vibrational modes of C_2F_6 beginning with ν_4 (8 meV), ν_{12} (27 meV), and ν_3 (43 meV) will be excited and together with rotational excitation contribute slightly to the 'elastic peak'. With the present energy resolution these cannot be resolved and are included in what is called the 'elastic peak' below. Mode ν_3 seems to contribute about 1.3%, cf figure 8. Such small contributions exert very little influence on the shape of the elastic peak. True superelastic features were not observed; such 'features' also appear occasionally in the He spectra. Some electrons with energies higher than the passing energy E_0 of the analyser may find their way into the channeltron by multiple reflection.

The observed counts of scattered electrons were converted into absolute cross sections by re-measurement of the known differential cross sections (DCS) of He (Boesten and Tanaka 1992) as described at length in the papers by Trajmar and Register (1984) and Brinkmann and Trajmar (1981). This implies adjustment of the gas-pressures for equal Knudsen numbers so that the gas beam profiles remain similar. The actual head pressures behind the nozzle were about 1 Torr for C_2F_6 and 7 Torr for He. We have used the pressure ratio formula for the conversion of the DCS. There have been persistent reports in the literature on non-linearities in plots of the flow-rate versus head pressure (Trajmar and Register 1984, Khakoo and Trajmar 1986, Alle *et al* 1992) even for simple gases like N_2. However, all these refer to capillary nozzles. We were not able to reproduce such non-linearities with our equipment, a simple tube nozzle, a Baratron and a flow controller acting as a flow meter (Nippon Tylan Corp.). Also note that flow meters need individual correction factors for every single gas.

The impact energy was calibrated against the 19.37 eV resonance of He and, for lower energies, against the ($\nu = 0 \rightarrow 1$) peak of N_2^- at an incident energy of 1.97 eV (Wong and Dubé 1978).

As mentioned, a single spherical analyser with virtual slits allows a few electrons with energies off E_0 to pass by reflection from the walls (see e.g. Froitzheim *et al* 1975). They form a long tail on the loss side of the elastic peak (about 0.3% or less of the elastic peak). The elastic peak of He together with this background can be represented rather well by the sum of a Gaussian peak (height 100%), the power of a Lorentzian distribution $(L_1)^4$ for the symmetric near-tails (height ≈3%) plus a very broad Lorentzian $(L_2)^{1.5}$ shifted from the elastic peak by about 10 FWHM (height ≈0.3%). The vibrational peaks of energy loss spectra ride on this background. We have developed an approximation to this background based on the measured FWHM and the estimated heights at 0.02 and 0.5 eV. The latter is almost uniquely determined by the tangent to the valleys of the loss spectra, the former must be found by trial and error, see below.

Direct experimental errors are estimated as 15–20% for DCS and 20–30% for vibrational excitation cross sections. The lower numbers have been used for the error bars of the plots.

2.2. *Extrapolation and integration of cross sections*

The measured elastic DCS were extrapolated to 0° and 180° to obtain the integrated (Q_I) and momentum transfer cross sections (Q_M) by numerical integration. Both Q_I and Q_M are quite stable under various extrapolations because they stress the experimental region through integration weights $\sin\theta$ and $(1-\cos\theta)\sin\theta$.

Extrapolations must fulfil the following requirements: (1) they must be good representations of the data, (2) they should be free of wiggles (systematic ± deviations from a presumed smooth curve), and finally (3) their integrated cross section Q_M and Q_I should form relatively smooth curves. Requirement (2) excludes direct Legendre fittings like

$$f(\theta)=\sum a_l P_l(\cos\theta) \qquad \text{or even} \quad \text{DCS}=\sum a_l P_l(\cos\theta) \tag{1}$$

which produce strong wiggles at 60 and 100 eV. We have therefore derived our fits by modification of the well known elastic and inelastic phaseshift fittings (Bransden 1970), because the compact shape of the molecule and averaging over its directions in space may result in an approximate spherical symmetry:

$$\begin{aligned} f(\vartheta)&=(2ik)^{-1}N_k\left(\sum_{l=0}^{L}(\eta_l e^{2i\delta_l}-1)(2l+1)P_l(\cos\vartheta)+C_L(\alpha,k,\vartheta)\right)\\ C_L(\alpha,k,\vartheta)&=2i\pi\alpha k^2\left(\tfrac{1}{3}-\tfrac{1}{2}\sin\tfrac{1}{2}\vartheta-\sum_{l=1}^{L}\frac{P_l(\cos\vartheta)}{(2l+3)(2l-1)}\right). \end{aligned} \tag{2}$$

Here α is the polarizability (42.02 au, Weast 1987) and k the wavenumber. The modifications consist of the addition of the Thompson correction $C_L(\alpha, k, \theta)$ for phases higher than the cutoff L (Thompson 1966), the introduction of a size-fitting parameter N_k (first proposed by Register *et al* 1980), and the removal of the constraint $\eta_l \leqslant 1$ for $l=0, 1, 2$. (We used $\eta_l \equiv 1$ for $l>2$, and for all fits below 15 eV.) Wiggle-free fits with $\eta_l \leqslant 1$, which could be found only for 10 and 15 eV, are almost indistinguishable from the proposed fits. Whenever the number of parameters exceeded the number of data we 'doubled' the data by geometric interpolation before fitting.

The following applies to the 60 eV example with $L=9$. The Thompson correction $C_L(\alpha, k, \theta)$ produces a sharp spike of size 15 Å^2 sr^{-1} at $\theta=0°$, riding on a flat, wave-like section (10° to 180°) of size 0.15 ± 0.15 Å^2 sr^{-1}. Partial waves near $l=\frac{1}{2}L$ help to

smooth this wave. $L \approx 9$ is required because of the steep descent of the data between 10° and 30°. Attempts to obtain a constrained fit ($\eta_l \leqslant 1$) to the unconstrained extrapolated DCS ($\eta_l > 1$)—usually a good trick to telescope the range—show systematic deviations in the *experimental* region. These deviations may reflect distortions arising from multicentre scattering.

The fits are not necessarily unique except for the lowest energies; they depend on the choice of L and the initial values of the fitting parameters. We have selected the fits according to the three criteria given above. Modified 'elastic' ($\eta_l \equiv 1$) and 'inelastic' fits were joined at 10 eV.

3. Results

3.1. Differential cross sections

The measured and normalized differential cross sections are displayed in figure 1 and listed in table 1. A three-dimensional view is given in figure 2. The much less reliable extrapolations have been included only because no theory presently exists, and repeated requests have been made by plasma modellers for our estimates at low and high angles. Modified inelastic fits were used up to 10 eV, just below the onset of electronic excitation at 11 eV (Robin 1974). The 10 eV plot of figure 1 demonstrates the smooth transition between the two types of fittings. The steep ascent toward $\theta = 0°$ in the 2 eV and 3 eV traces may give the impression of an artifact from the Born-derived Thompson correction of equation (2). However a very similar shape has actually been measured in the experimental region for CH_4 (Boesten and Tanaka 1991).

Similar DCS have quite recently been obtained by the Kaiserslautern group (Merz 1993, preliminary plots) for 2–10 eV and 15–90°. As far as we know they use a flow meter in their He normalization. So far, the differences between their and our data seem to be of order ±20%.

In figure 3 we present a comparison of the elastic DCS with previous measurements of the similar molecule C_2H_6 (Tanaka *et al* 1988, same instrument). The size of the cross sections is similar. At low energies, the hexafluoroethane spectra seem to have been pulled in toward smaller angles, while at higher energies, the ethane spectra look smoother. The larger F atom increases the size of the molecule—and thus the need for higher partial waves in a Legendre expansion. The valley at 40° in the 30 eV of C_2F_6 spectrum (figure 1(*a*)) is much more pronounced than that in C_2H_6, and the three-dimensional plot of C_2F_6 displays many more features than a similar plot of C_2H_6.

3.2. Total elastic and momentum transfer cross sections Q_I and Q_M

Q_I and Q_M were obtained by numerical integration of the fits with weights $\sin\theta$ and $\sin\theta\,(1-\cos\theta)$. They are included at the bottom of table 1 and are plotted in figure 4. Their accuracies are estimated to be about 25% for Q_I and 30–35% for Q_M. At low energies they are mainly determined by the experimental region, at 20–30 eV the extrapolated sections contribute about 35–40% to the integrals, and at 100 eV, the extrapolated sections contribute about 50%. From past experience with fitted extrapolations, the shape of Q_M should resemble that of Q_I more closely. The fits (and theories for other gases) have steeply rising sections near 0° and 180°, and much of the contribution to Q_M arises from the steep tail in the extrapolated region beyond 140°. The

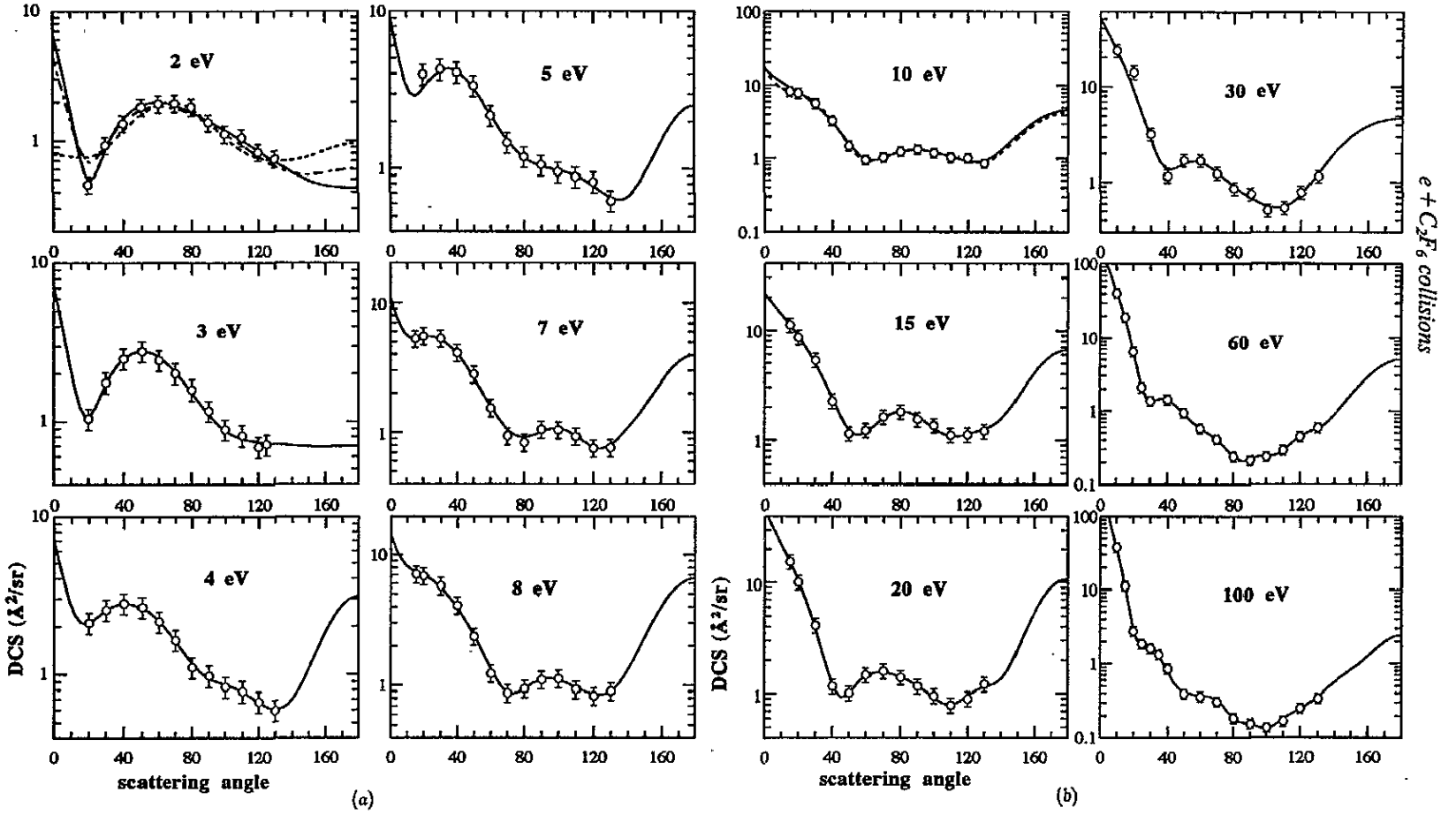

Figure 1. Elastic DCS. (*a*) 2–8 eV: modified phaseshift fitting (——). The 2 eV plot includes unmodified phaseshift fitting without (- - - - -) and with (·—·—·) the Thompson correction for higher phases; see equation (2). The integrated cross sections Q_I and Q_M of all three traces agree within 5%. (*b*) 10–100 eV: modified *inelastic* phaseshift fitting (——), see text. The broken curve in the 10 eV trace was obtained by modified phaseshift fitting as for (*a*). The fits are intended as a basis for obtaining the much more stable integrals of figure 4.

Table 1. Elastic DCS in $Å^2\,sr^{-1}$ and integrated cross sections Q_I and Q_M in $Å^2$.

deg	2 eV	3 eV	4 eV	5 eV	7 eV	8 eV	10 eV	15 eV	20 eV	30 eV	60 eV	100 eV
10										23.54	41.13	37.91
15					5.304	7.050	8.261	11.28	15.45		19.31	11.26
20	0.4578	1.042	2.113	3.963	5.536	6.882	7.803	8.700	10.09	14.07	6.473	2.772
25											2.092	1.859
30	0.9265	1.758	2.562	4.269	5.332	5.772	5.676	5.326	4.126	3.220	1.373	1.607
40	1.368	2.496	2.805	4.089	4.127	4.094	3.322	2.269	1.174	1.154	1.428	0.8559
50	1.837	2.772	2.660	3.365	2.797	2.370	1.487	1.146	1.015	1.694	0.9475	0.3984
60	1.952	2.439	2.160	2.191	1.549	1.228	0.9494	1.230	1.477	1.681	0.5767	0.3622
70	1.960	2.018	1.650	1.471	0.9424	0.8760	1.033	1.633	1.598	1.239	0.4094	0.3113
80	1.838	1.591	1.109	1.190	0.8390	0.9448	1.243	1.813	1.405	0.8628	0.2396	0.1880
90	1.394	1.168	0.9805	1.058	1.060	1.107	1.328	1.551	1.172	0.7576	0.2132	0.1566
100	1.132	0.8898	0.8343	0.9543	1.047	1.125	1.187	1.365	0.9623	0.5131	0.2386	0.1387
110	1.066	0.8162	0.7842	0.8861	0.9339	0.9334	1.034	1.114	0.7965	0.5407	0.2924	0.1694
120	0.8144	0.6880	0.6748	0.8246	0.7572	0.8326	1.010	1.124	0.9013	0.7836	0.4476	0.2530
130	0.7224	0.7152	0.5981	0.6253	0.7671	0.9042	0.8516	1.209	1.227	1.148	0.5915	0.3439
Q_I	15.53	17.61	19.11	21.19	22.66	24.26	24.88	28.04	28.09	25.33	21.51	16.12
Q_M	12.98	13.18	14.11	14.56	16.43	17.85	18.81	22.73	22.45	18.93	10.62	5.86

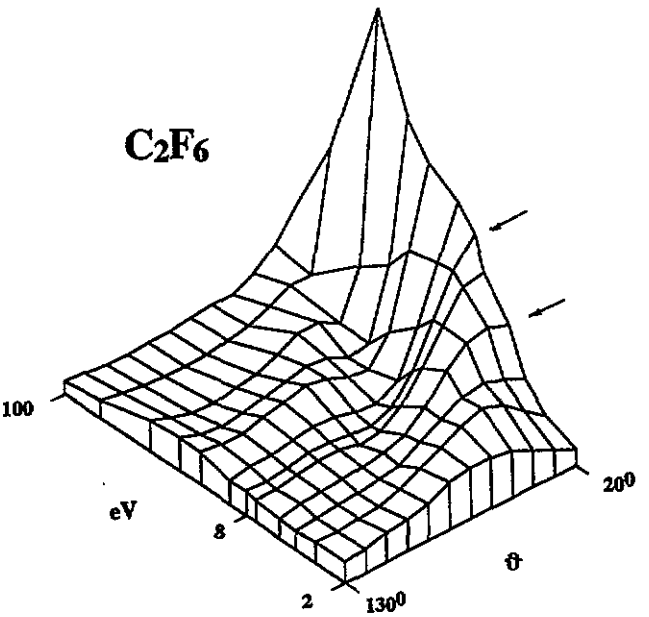

Figure 2. Three-dimensional view of the DCS of figure 1. The arrows indicate the position of the vibrational resonance enhancements near 4.5 and 8 eV. Some faint, angle-independent ridges are discernible.

elevated peak of Q_M compared with Q_I could easily be reduced by about 15% if the tail were less steep. The discrepancy in shape may reflect a limitation of our fitting function. Q_I is less strongly affected by the tail because of the different integration weight.

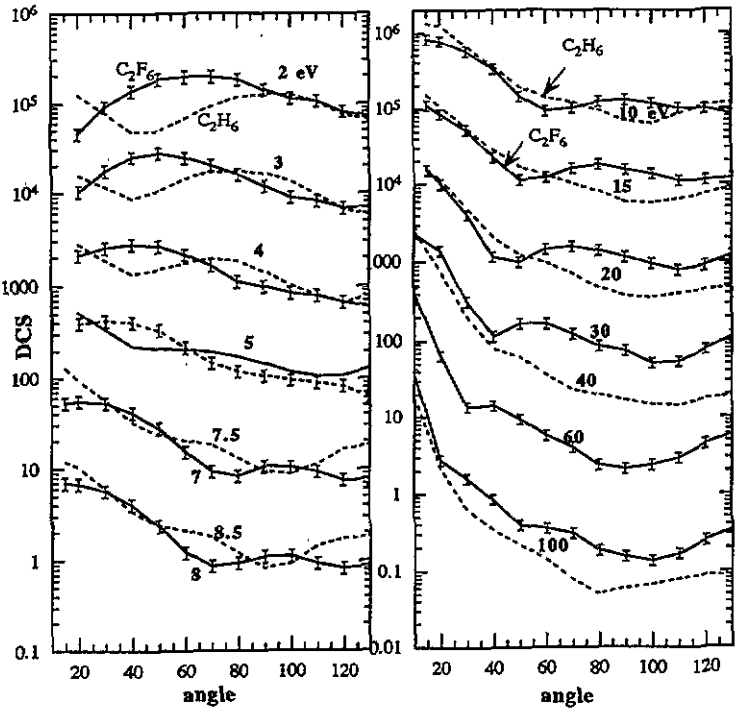

Figure 3. Comparison of the elastic DCS of C_2F_6 and C_2H_6 (Tanaka *et al* 1988).

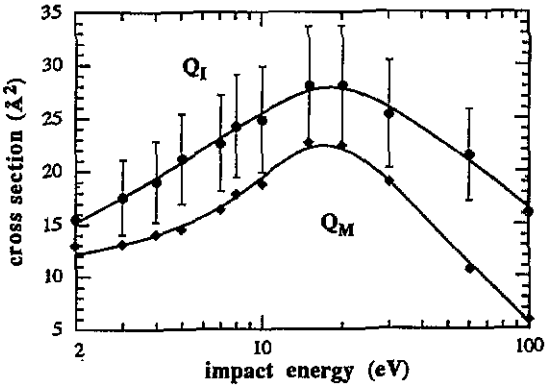

Figure 4. Integrated elastic (Q_I) and momentum transfer (Q_M) cross sections as obtained by numerical integration under the extrapolated fits of figure 1.

No directly comparable experimental data exist in the literature. The older estimates of Q_M from 0.01 to 1000 eV by Hayashi (1987) agree at the lower energies (90% of our estimates), but they peak at around 7 eV (80%) and drop off faster toward 100 eV (60%). Similarly, a calculation of Q_M from the swarm measurements of Hunter and Christophorou (1985) by Pirgov and Stefanov (1990) up to 8 eV shows a peak at 4 eV (12.3 Å^2) which is close to our value, but then the calculation drops off fast toward 8 eV (6.5 Å^2).

3.3. Vibrational excitation

Figure 5 shows some of the many vibrational loss spectra taken for C_2F_6. A small enhancement of the 0.16 eV peak—for simplicity called the stretching peak, ν_s—can be observed at 4.5 eV and at 8.5 eV. The two enhancements are echoed in small ridges marked by arrows in the three-dimensional plot, figure 2. The 4 eV trace contains large harmonics, a feature not found in C_2H_6.

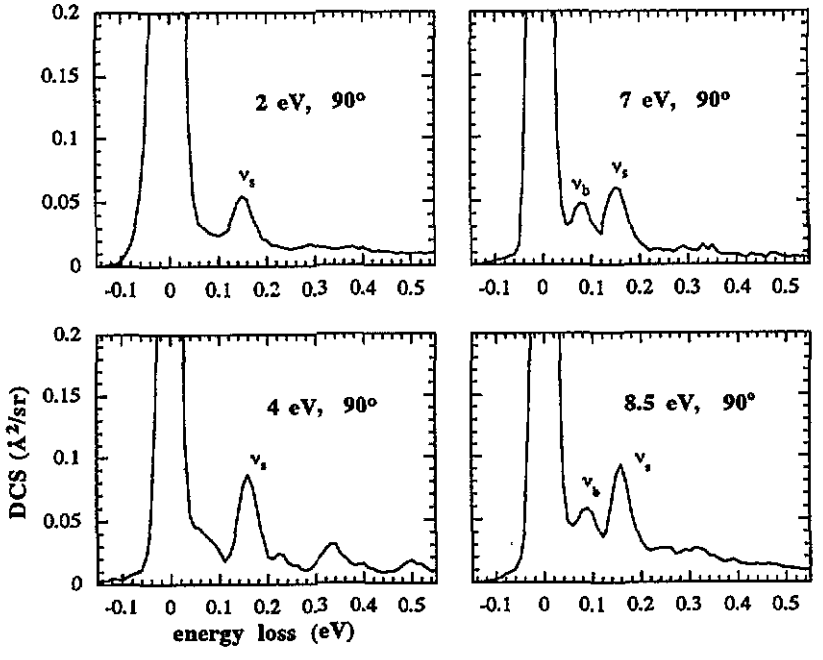

Figure 5. Various energy loss spectra for a scattering angle of 90°, ν_s = stretching peak, ν_b = bending peak. The larger peak ν_s consists mainly of vibrational mode ν_1.

Excitation functions for the 0.16 eV energy loss stretching mode were recorded at four differential angles (figure 6). These spectra are normalized point by point to those of He. Note the different scales, and, in comparisons with figures 5 or 7, the inclusion or exclusion of the background signal. At forward scattering angles, weak features ride on the descending trace of direct scattering. At larger angles, a narrower peak at 4.3 eV and a broader peak at 8.5 eV compete with one another. A wide and slightly asymmetric resonance has also been observed in C_2H_6 at 7.5 eV (Boesten *et al* 1990), but not the narrower feature at lower energies. The slight angle dependence of the enhancements of C_2F_6 may be an instrumental effect.

The angular behaviour of ν_s at the minima and maxima of figure 5 is shown in figure 7. The traces were obtained by subtracting the local background from both ν_s and the elastic peak of plots like figure 5, and then forming the ratio of the areas contained within ±0.02 eV of the peak. The main contribution to peak ν_s consists of the totally symmetric vibration mode ν_1, and thus the angular behaviour of figure 7 mainly reflects this mode. The 2 eV trace shows typical Born-like behaviour (direct scattering), and at larger angles the 8.5 eV trace, and possibly the 4 eV trace too, resemble Legendre polynomials. The 7 eV trace is essentially flat, with a very small

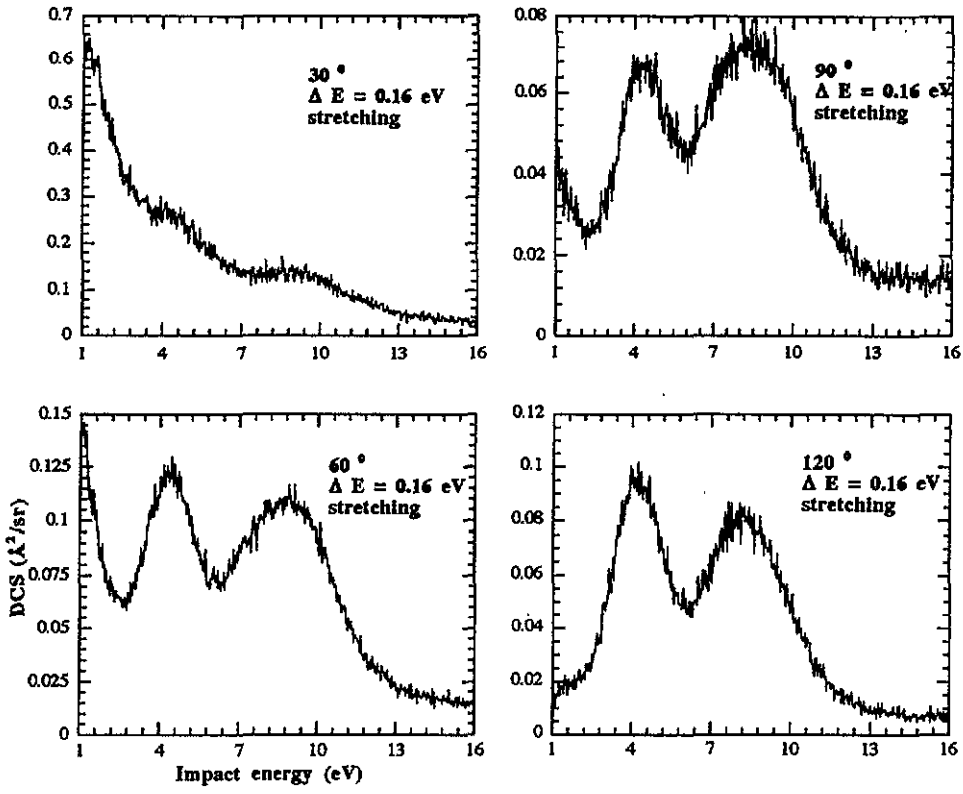

Figure 6. Excitation functions of the loss peak v_s of figure 5. The traces are normalized channel by channel to the DCS of He.

wave-like pattern symmetrically around 90°. This pattern may be part of the 4 eV feature, because the minimum of figure 6 is rather shallow.

A more thorough discussion of these enhancements is given in the following section.

4. Discussion

Symmetry analyses for the similarly structured C_2H_6 and Si_2H_6 were published previously (Boesten *et al* 1990, Dillon *et al* 1994). The main results are repeated in table 2 and equation (3). We have performed some GAUSSIAN-92 calculations (Frisch 1992) with STO-3G and other basis sets up to RHF/6-31G*, and the experimental geometry of C_2F_6 as given in table 5, which consistently produce lower virtual orbitals of symmetry species e_u (6.656 eV) and a_{2u} (9.730 eV) followed by a_{1g} with 9.834 eV in the 6-31G basis set. Martell and Boyd (1992) report an inverted order of a_{1g} (8.8838 eV) and a_{2u} (8.9437 eV) for their MP2/6-311G* set with a geometry optimized by a Gaussian calculation. Species e_u and a_{2u} were the symmetry species assumed for the temporary negative ion (TNI) of C_2H_6. The vibrational modes that can possibly be enhanced by electron trapping are listed in table 2 and described in table 3. In the last three entries of table 3, the carbon atoms move only orthogonally to the C–C bond.

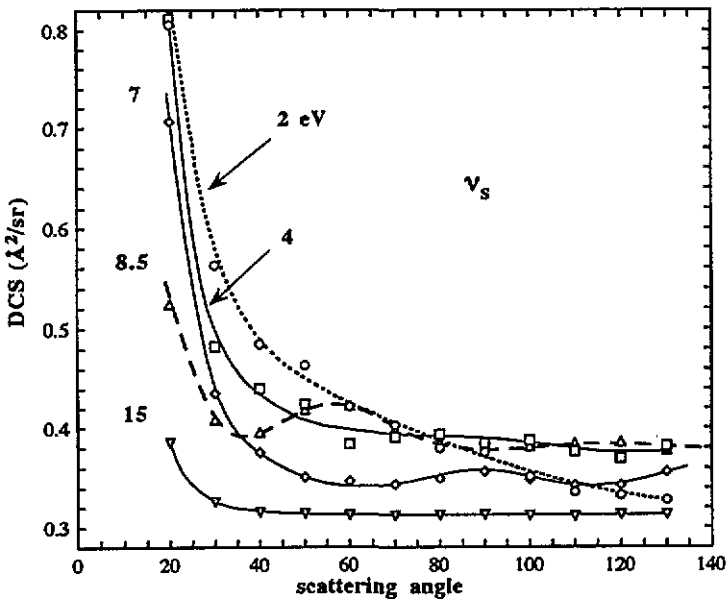

Figure 7. Angular behaviour of peak ν_s of figure 5 at various incident electron energies. The local background was subtracted from the energy loss spectra, as in figure 5, before data were transferred into figure 7. Error bars have been omitted for clarity. Relative errors are about 10%, absolute errors are larger (20–30%).

Table 2. Representations of the symmetry species of the states involved in resonance.

	Representations				
Assumed trapping state	a_{2u}		e_u		(a_{1g})
Final vibrational state	a_{1g}	a_{1g}	or	e_g	a_{1g}
Corresponding vibrational modes	ν_1, ν_2, ν_3	ν_1, ν_2, ν_3		$\nu_{10}, \nu_{11}, \nu_{12}$	ν_1, ν_2, ν_3
Electron wave	a_{2u}	e_u		a_{1u}, a_{2u}, e_u	a_{1g}
l in the molecular frame	1, 3	1, 3		1, 3, 5	0, 2

Table 3. Description of the allowed vibrational frequencies†.

Symmetry species	Vibrational mode	ΔE (eV)	Long description
a_{1g}	ν_1	0.1523	3 C–F elongations + C–C contraction
	ν_2	0.1001	FCC angle increase + C–C contraction
	ν_3	0.0432	CF_3–CF_3 stretch
e_g	ν_{10}	0.1551	2 CF-elongations + 1 CF contraction
	ν_{11}	0.0645	F–F contraction + 1 CF elongation
	ν_{12}	0.0273	2 FCC angle decreases + 1 FCC angle increase

† The descriptions refer to one block of CF_3 and are derived from plots of Herzberg (1944, p 115). The National Bureau of Standard Tables (Shimanouchi 1972) give the symmetry species of ν_{10}–ν_{12} as e_u.

The 8.5 eV angular distribution of figure 7 is slightly reminiscent of a Legendre polynomial of order $k=6$. According to angular correlation theory (Andrick and Read 1971), the angular part of the cross sections can be expanded as a Legendre series of form

$$W(k_i, k_f) = \sum_k A_k P_k(\cos \vartheta)$$

with

$$A_k = \sum \sum_q A_q \begin{pmatrix} l_1 & l_1' & k \\ 0 & 0 & 0 \end{pmatrix} \begin{pmatrix} l_2 & l_2' & k \\ 0 & 0 & 0 \end{pmatrix}. \tag{3}$$

Here the first sum is over $l_1 l_1' l_2 l_2'$. For details, the reader is referred to our paper on CF_4 (Boesten *et al* 1992). The Clebsch–Gordan coefficients require $l + l' - k \geqslant 0$ in the molecular frame for incoming waves (l_1) and outgoing waves (l_2); thus either $l_1 = l_2 = 3$, or $l_1 = 4$, $l_2 = 2$. The latter are excluded from table 2 if one stresses the similarity to C_2H_6 and low-order l. Unfortunately, $l_1 = 3$ does not help to distinguish possible resonant states a_{2u} and e_u, and the 4 eV angular distribution is yet less pronounced ($k=8$, $l_1 = 5$, $l_2 = 3$ or vice versa?).

We have therefore tentatively assumed that the only frequencies that can be enhanced by a TNI are those of table 3 and have performed wave decompositions on the energy loss spectra at 4 and at 8.5 eV, one for ν_1–ν_3, a second for ν_{10}–ν_{12}, and a third for all six frequencies combined. Some samples are shown in figure 8 and table 4. The apparatus function was derived from He measurements as described above and a non-linear background, estimated by a two-parameter fit as mentioned above, was subtracted. The height at 0.02 eV was determined by trial and error in combination with low-range decomposition. It is not too crucial since our aim is a shape analysis and not a height analysis. For a given set of allowed vibrational modes we produce a list of all energies which can be constructed from up to four frequency combinations and determine their relative weights in a least squares fit over the lower range from ν_3 to ν_1 where the fits become nearly unique (the spectra for decomposition are recorded at high counting rates to reduce the influence of noise). The fitting range is then extended to all peaks of interest by including higher harmonics as needed, preferably simple combinations. This choice is more arbitrary. The long range decomposition serves only as a check for possible trends and to identify major contributions to the larger loss peaks. The sensitivity in energy is surprisingly high, a few meV off the correct energy usually produces very poor local fits.

The decomposition attempts can be summarized as follows. The 8.5 eV set needs ν_{11} for a good fit at 0.05 eV (min.) and 0.08 eV (max.), and decompositions using only ν_{10}–ν_{12} fail. The trace also seems to contain some small overtones of ν_{10}. If the observed vibrational enhancement is due to a single TNI as was assumed in the derivation of table 2, the requirement of ν_{10} or ν_{11} would be indicative of e_u. A similar conclusion was previously obtained for C_2H_6. The 4 eV trace shows large harmonics that can be fitted closely by frequencies ν_1–ν_3 alone, all of which imply a C–C stretch (see table 3). The stretching peak ν_s includes a large contribution of ν_3, and the harmonics seem to contain overtones of ν_3. However, at 0.065 eV, and only here, ν_{11} is needed. If we assume that ν_{11} is due to a small incipient deformation of the molecule by the incoming electron, the resonance could be explained entirely by an electron capture into a TNI of species a_{2u}, the σ^* C–C molecular orbital.

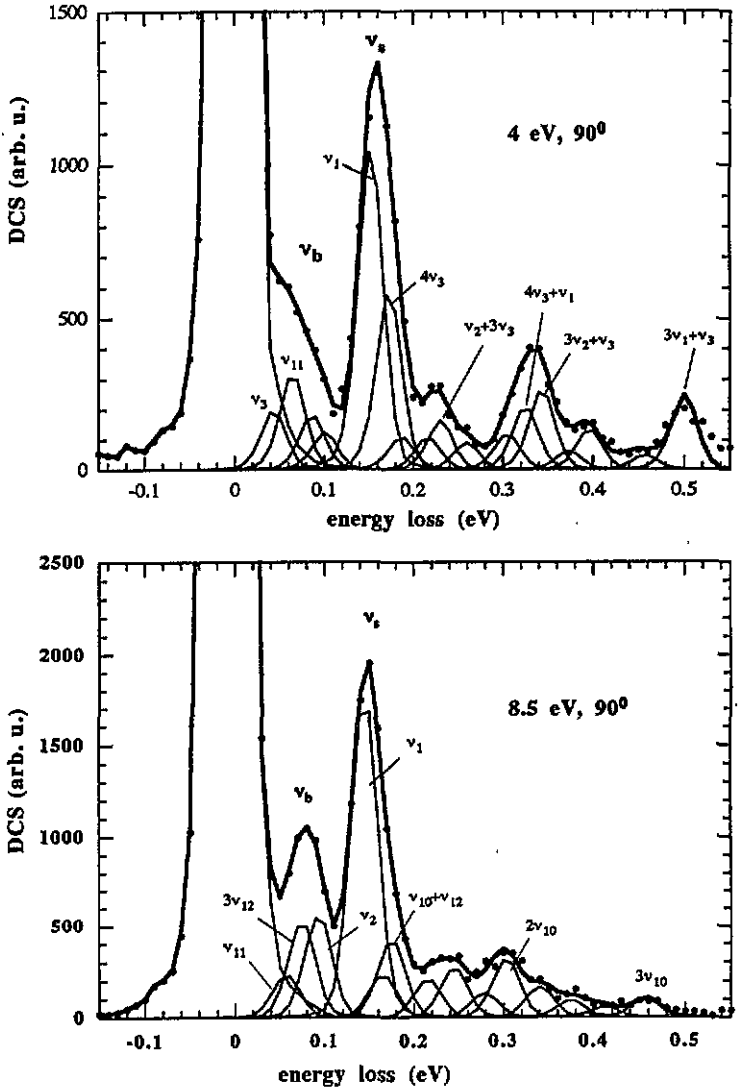

Figure 8. Decomposition of the energy loss spectra at the two vibration-enhancing incident energies. According to a symmetry species analysis, we have considered only modes ν_1–ν_3 and ν_{10}–ν_{12}. The relative intensities of the single peaks are listed in table 4. (Because of limitations in the plotting software, decomposed peak $[2\nu_1+3\nu_3]$ of the 4 eV spectrum is not shown.)

Indirect confirmation of these assignments can be derived from dissociative electron attachment measurements (peaks at 4 eV, Spyrou *et al* 1983), from cross sections derived by high-pressure swarm techniques (peak at 4 eV, Hunter and Christophorou 1984; see figure 9), and from electron transmission experiments (Ishii *et al* 1988). The latter observed peaks at 4.60 and 8.86 eV and explained the shift with respect to Spyrou *et al* as being due to differences in the survival probability of the anions at both ends of the energy band (Ishii *et al* p 2117). These authors tried to associate the energy of virtual orbitals (STO-3G-basis HF calculation, e_u: −12.73 eV, a_{2u}: −13.24 eV, a_{2u}:

Table 4. Relative sizes of the decomposition† spectra at 90°.

4 eV			8.5 eV		
Mode	eV	Size (%)	Mode	eV	Size (%)
Elastic	0	100	Elastic	0	100
ν_3	0.0432	1.27	ν_{11}	0.0645	0.78
ν_{11}	0.0645	2.07	$3\nu_{12}$	0.0818	1.76
$2\nu_3$	0.0863	1.18	ν_2	0.1001	1.88
ν_2	0.1001	0.80	ν_1	0.1523	5.96
ν_1	0.1523	6.83	$4\nu_3$	0.1726	0.79
$4\nu_3$	0.1726	3.82	$\nu_{10}+\nu_{12}$	0.1824	1.42
$2\nu_3+\nu_2$	0.1864	0.72	$\nu_1+\nu_3+\nu_{12}$	0.2227	0.71
$5\nu_3$	0.2156	0.70	$\nu_1+\nu_2$	0.2523	0.92
$3\nu_3+\nu_2$	0.2295	1.06	$2\nu_2+2\nu_3$	0.2864	0.45
$6\nu_3$	0.2589	0.59	$2\nu_{10}$	0.3102	1.07
$2\nu_1$	0.3045	0.77	$\nu_3+2\nu_2$	0.3477	0.57
$4\nu_3+\nu_1$	0.3249	1.38	$3\nu_{12}+3\nu_2$	0.3821	0.32
$\nu_3+3\nu_2$	0.3434	1.72	$4\nu_2$	0.4003	0.06
$4\nu_3+2\nu_2$	0.3727	0.40	$4\nu_{12}+2\nu_{10}$	0.4194	0.19
$\nu_3+\nu_1+2\nu_2$	0.3956	0.88	$3\nu_{10}$	0.4654	0.36
$3\nu_3+2\nu_1$	0.4340	0.23			
$3\nu_1$	0.4568	0.32			
$\nu_3+3\nu_1$	0.5	1.58			

† The decompositions are unique only up to about 0.15 eV.

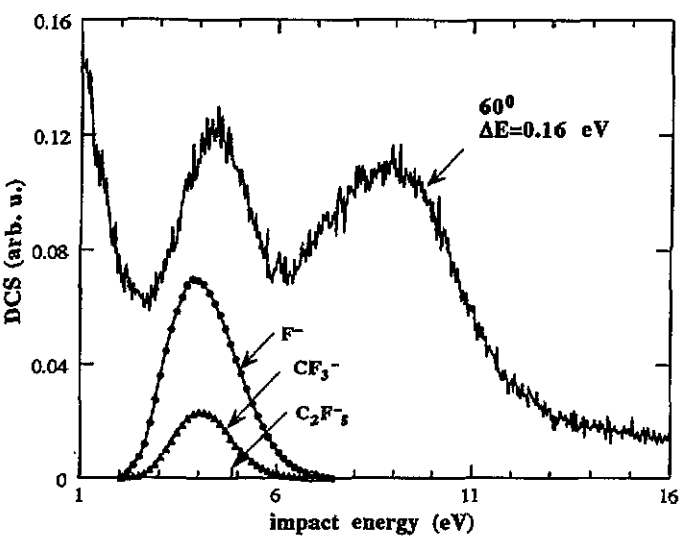

Figure 9. Comparison of our excitation with dissociative attachment cross sections (Spyrou *et al* 1983). The traces of F^- and CF_3^- are scaled correctly between themselves; the peak of $C_2F_5^-$ is too small to be shown (size = 1/1000 of F^-).

−15.65 eV) with their observed resonance energies by lining up −4.60; −8.86 eV and the shifted orbital energies −3.73 (e_u); −4.24 (a_{2u}); −6.65 (a_{2u}). Taken literally, this association would be the opposite of our interpretation; the association may be influenced by their discussion of inner-shell spectra.

Some controversial attempts have been made to establish a statistical correlation between the shape resonance energy of inner-shell energy loss spectra and the corresponding molecular bond lengths (Hitchcock *et al* 1984, Hitchcock and Stöhr 1986 vs Piancastelli *et al* 1986, Sette *et al* 1984). In spite of obvious differences in the potential because of the additional electron in our case, these inner shell shape resonances involve molecular σ^* valence orbitals similar to or even the same as our TNI (cf Dehmer and Dill 1979). Others have investigated a statistical connection between electron affinity and virtual orbital energies (ε_{LUMO}) for similarly structured molecules (Heinrich *et al* 1986, also see Chen and Gallup (1990) for some theoretical criteria for selecting among the virtual orbitals). Unfortunately, none of these studies includes C_2F_6.

We have therefore compiled a few relevant data for CF_4 and C_2F_6 and the similarly structured CH_4 and C_2H_6 molecules in table 5. The C–X bond lengths change by less

Table 5. Bond lengths, XCX angles and vibrational resonance energies[a].

	Bond lengths (au)				Vibrational resonance energy
	C-H	C-F	C-C	α (deg)	(eV)
CH_4	1.0870	—	—	109.5	7.5
CF_4	—	1.323	—	109.5	8; 21 (small)
C_2H_6	1.0940	—	1.5351	111.2	8
C_2F_6	—	1.326	1.545	109.8	4.3; 8.6

[a] Data from Nihon-Kagakkai (1984).

than 0.6% with the addition of another carbon atom, as does the C–C bond upon fluorination. We can imagine the temporarily trapped electron as a particle in a box of approximate width C–C. The vibrational resonance shifts slightly up from CH_4 to C_2H_6 (7%), and so one would expect a similar trend for CF_4 and C_2F_6 (7.5%). That is, the 8.5 eV resonance of C_2F_6 corresponds to the 8 eV resonance of CF_4. On the other hand, the 8 eV resonance in CF_4 can be explained only by temporary electron capture into a C–F antibonding orbital (e_u in C_2F_6) and a lower-lying resonance does not exist. Thus, the 4 eV resonance in C_2F_6 most likely involves orbitals not found in CF_4, such as a C–C orbital, or a_{2u}. There is no low-energy resonance in C_2H_6.

According to Spyrou *et al* (1983), the TNI at 8.5 eV in C_2F_6 does not lead to a measurable dissociative attachment (ion lifetime $>10^{-6}$ s). This may be explained by an inspection of figure 6 in terms of energy spread. Assuming that the small 4 eV peak rides on a broad 8 eV peak similar to those observed in other C_2X_6 measurements, we obtain $\Delta E_4 \approx 1.9$ eV and $\Delta E_8 \approx 4$–5 eV. The unfolded CF_3-peak of Spyrou *et al* has a width of 1.7 eV, and its raw width is 1.9 eV. Translated into lifetimes according to $\Delta\tau \geqslant h/\Delta E$ (not $\hbar/\Delta E$†), we obtain $\Delta\tau_4 = 2\times10^{-15}$ s and $\Delta\tau_8 = 8\times10^{-16}$ s. Note that Spyrou *et al* calculate a mean autodetachment time of the TNI as 1.74×10^{-15} s from their swarm experiments with the help of semiclassical formulae. One could then argue (see, e.g. Gallup 1993, equation (32)) that $\Delta\tau_8 = 8\times10^{-16}$ s is too short a lifetime to lead to dissociation, when compared with the period of vibration, $\tau = 2.7\times10^{-14}$ s.

† Usually the uncertainty is given as $\Delta\tau \geqslant \hbar/\Delta E$ (e.g. Schiff 1968, p 3). However, its derivation depends on the arbitrary definition of the breadth of a wavepacket. For example, Kompaneyets (1961) defined the uncertainty as $\Delta\tau \geqslant 2\pi\hbar/\Delta E$. Here we have arbitrarily selected the compromise $\Delta\tau \geqslant h/\Delta E$ because it produces more realistic estimates in the present case.

5. Conclusion

In the present investigation, we are providing for the first time a compilation of low-energy elastic differential cross sections for e–C_2F_6 collisions, together with an estimate of the integrated cross sections Q_I and Q_M. We were able to demonstrate that fluorination of C_2H_6 produces a TNI enhancement of vibrational excitation at energies below the well-known broad resonance of saturated carbons in the neighborhood of 8 eV. What is needed now is a theoretical investigation of the scattering process as well the inner-shell excitations under the common aspect of electrons trapped temporarily in a valence orbital of the molecule. At present, we do not know even the LUMO orbitals, except for a guess from the variationally unstable virtual orbitals of a Gaussian calculation. A theoretical treatment may also be able to determine whether there should be a third vibrational enhancement near 22 eV, as was previously observed in CF_4†.

References

Alle D T, Gulley R J, Buckman S J and Brunger M J 1992 *J. Phys. B: At. Mol. Opt. Phys.* **25** 1533–42

Andrick D and Read F H 1971 *J. Phys. B: At. Mol. Phys.* **4** 389–96

Arai S, Watanabe T, Ishikawa Y, Oyama T, Hayashi O and Ishii T 1984 *Chem. Phys. Lett.* **112** 224–7

Boesten L and Tanaka H 1991 *J. Phys. B: At. Mol. Opt. Phys.* **24** 821–32

—— 1992 *At. Data Nucl. Data Tables* **52** 25–42

Boesten L, Tanaka H, Kobayashi A, Dillon M A and Kimura M 1992 *J. Phys. B: At. Mol. Opt. Phys.* **25** 1607–20

Boesten L, Tanaka H, Kubo M, Sato H, Kimura M, Dillon M A and Spence D 1990 *J. Phys. B: At. Mol. Opt. Phys.* **23** 1905–13

Božin S E and Goodyear C C 1968 *J. Appl. Phys.* D **1** 327–34

Bransden B H 1970 *Atomic Collision Theory* (New York: Benjamin) Ch I

Brinkmann R T and Trajmar S 1981 *J. Phys. E: Scr. Instrum.* **14** 245–54

Buckley B D 1977 *J. Phys. B: At. Mol. Phys.* **10** L351–5

Chen D and Gallup G A 1990 *J. Chem. Phys.* **93** 8893–901

Dehmer J L and Dill D 1979 *Electron-Molecule and Photon-Molecule Collisions* ed T Rescigno and V McKoy (New York: Plenum Press) pp 225–65 (see also: I Shimamura and M Matsuzawa (eds) 1979 Connections between molecular photoionization and electron–molecule scattering with emphasis on shape resonances *Symp. on Electron–Molecule Collisions* (Tokyo: University of Tokyo))

Dillon M A, Boesten L, Tanaka H, Kimura M and Sato H 1994 *J. Phys. B: At. Mol. Opt. Phys.* **27** 1209–19

Fisk G A 1978 *Chem. Phys. Lett.* **60** 11–5

Frisch M J *et al* 1992 GAUSSIAN 92 Revision E1 (Pittsburgh, PA: Gaussian Inc.)

Froitzheim H, Ibach H and Lehwald S 1975 *Rev. Sci. Instrum.* **46** 1325–8

Gallup G A 1993 *J. Phys. B: At. Mol. Opt. Phys.* **26** 759–74

Haond M 1992 *Eur. Pat. Appl. EP* **487** 380

Hayashi M 1985 *Swarm Studies and Inelastic Electron–Molecule Collisions* ed L C Pitchford, B V McKoy, A Chutjian and S Trajmar (New York: Springer) pp 167–87

Hayashi M 1987 *Gaseous Dielectrics V (Proc. 5th Int. Symp. on Gaseous Dielectrics, Knoxville, TN)* ed L G Christophorou and D W Bouldin (New York: Pergamon) pp 27–33

Heinrich N, Koch W and Frenking G 1986 *Chem. Phys. Lett.* **124** 20–25

Herzberg G 1944 *Molecular Spectra and Molecular Structure* vol 2 (New York: Van Nostrand)

Hitchcock A P, Beaulieu S, Steel T, Stöhr J and Sette F 1984 *J. Chem. Phys.* **80** 3927–35

Hitchcock A P and Stöhr J 1986 *J. Chem. Phys.* **87** 3253–5 (Comment)

Hunter S R and Christophorou L G 1984 *J. Chem. Phys.* **80** 6150–64

Iriyama Y and Yasuda H 1992 *J. Polym. Sci.* A **30** 1731–9

† After completion of this manuscript, a weak wide peak was actually observed at 21 eV.

Ishii I, McLaren R, Hitchcock A P, Jordan K D, Choi Y and Robin M B 1988 *Can. J. Chem.* **66** 2104–21
Khakoo M A and Trajmar S 1986 *Phys. Rev.* A **34** 138–45
Kompaneyets A S 1961 *Theoretical Physics* (Moscow: Foreign Languages Publishing House)
Lee L C, Phillips E and Judge D L 1977 *J. Chem. Phys.* **67** 1237–46
Martell J M and Boyd R J 1992 *J. Phys. Chem.* **96** 6287–90 and private communication
Merz R (and Linder F) 1993 Private communication (see also *1993 Proc. XVIIIth Int. Conf. on Physics of Electronic and Atomic Collisions*) (Aarhus) p 301
Miller P A and Greenberg K E 1992 *Appl. Phys. Lett.* **60** 2859–61
Morris R A, Patrissi C J, Sardella D J, Davidovits P and McFadden D L 1983 *Chem. Phys. Lett.* **102** 41–4
Naidu M S and Prasad A N 1972 *J. Phys.* D **5** 983–93
Nihon-Kagakkai (ed) 1984 *Kagakubinran* vol 2 (Tokyo: Maruzen) pp 654–60 (in Japanese)
Op de Beeck M, Goethals M and Van den hove L 1992 *J. Electrochem. Soc.* **139** 2644–53
Piancastelli M N, Lindle D W, Feretti T A and Shirley D A 1986 *J. Chem. Phys.* **87** 2765–71 (3255–6 Reply)
Pirgov P and Stefanov B 1990 *J. Phys. B: At. Mol. Opt. Phys.* **23** 2879–87
Pirozhnaya L N, Zubkova O B and Gribov L A 1985 *Zh. Prikl. Spektrosk.* **43** 440–5
Register D F, Trajmar S and Srivastava S K 1980 *Phys. Rev.* A **21** 1134–51
Reinhardt K 1992 *Proc. Electrochem. Soc.* **92** 133–43
Robin M B 1974 *Higher Excited States of Polyatomic Molecules* vol 1 (New York: Academic) p 188
Senhorst H A J 1991 *Sci. Tech. Aerosp. Rep.* **29** Abstract no N91-22862
Sette F, Stöhr J, and Hitchcock A P 1984 *J. Chem. Phys.* **81** 4906–14
Shimanouchi T 1972 *Tables of Molecular Vibrational Frequencies, Consolidated* vol 1 (NSRDS-NBS 39) (Washington, DC: US Govt Printing Office)
Spyrou S M, Sauers I and Christophorou L G 1983 *J. Chem. Phys.* **78** 7200–16
Schiff L I 1968 *Quantum Mechanics* (Tokyo: McGraw-Hill Kogakusha) pp 3, 8
Tanaka H, Boesten L, Matsunaga D and Kudo T 1988 *J. Phys. B: At. Mol. Opt. Phys.* **21** 1255–63
Tanaka H, Boesten L, Sato H, Kimura M, Dillon M A and Spence D 1990 *J. Phys. B: At. Mol. Opt. Phys.* **23** 577–88
Thompson D G 1966 *Proc. R. Soc.* A **294** 160–74
Trajmar S and Register D F 1984 *Electron–Molecule Collisions* ed I Shimamura and K Takayanagi (New York: Plenum) pp 427–93
Weast R C 1987 *Handbook of Chemistry and Physics* (Boca Raton: CRC Press) Section E-64
Wong S F and Dubé L 1978 *Phys. Rev.* A **17** 570–6